Journal of
Polymer Materials

Tech Science Press

https://doi.org/10.32604/jpm.2026.081141

ARTICLE

Molecular Design of a Hyperbranched Polymer Wetting Agent for Superior Barite Sag Control in Ultra-Low Oil-to-Water Ratio Drilling Fluids

Dapeng Zou[1,2] **and Jun Wang**[1,*]

[1]College of Chemistry and Chemical Engineering, Northeast Petroleum University, Daqing, China
[2]Drilling Fluid Company, Daqing Drilling & Exploration Engineering Corporation, Daqing, China

*Corresponding Author: Jun Wang. Email: wangjun1965@yeah.net

Received: 24 February 2026; Accepted: 13 May 2026; Published: 30 June 2026

ABSTRACT: Reducing the oil-to-water ratio (OWR) of oil-based drilling fluids (OBDFs) to ultra-low levels (e.g., 55:45) exacerbates barite sag—a failure mode driven by barite's inherent hydrophilicity and the weakened suspending capacity of the oil phase. Conventional low-molecular-weight wetting agents fail under these demanding conditions due to weak adsorption and thermal instability. In direct response to the solid-phase control challenge described above, we designed and synthesized a new hyperbranched polymeric wetting agent (HP-Wet) via a deliberate molecular topology strategy. The HP-Wet architecture incorporates phosphonate groups for robust anchoring onto barite surfaces and long alkyl chains to confer oleophilicity. By optimizing the amine-to-anhydride molar ratio, HP-Wet-1.05 was obtained, exhibiting a well-defined hyperbranched structure with a moderate molecular weight (M_w = 31,021 g/mol) and narrow dispersity (PDI = 1.96). This agent demonstrated exceptional efficiency in barite wettability reversal, increasing the water contact angle from 21.9° to over 117.1°. In an ultra-low OWR (55:45) OBDF formulated with the synergistic cetyltrimethylammonium bromide (CTAB) system, the HP-Wet delivered outstanding comprehensive performance after dynamic aging at 180°C: superior sag resistance (sag factor = 0.505), high electrical stability (demulsification voltage > 1000 V), and low high-temperature/high-pressure fluid loss (1.5 mL), significantly outperforming a commercial wetting agent (X-407). The enhanced performance is attributed to a multi-scale stabilization mechanism distinct from interfacial emulsification: strong multi-point anchoring on barite at the molecular level; formation of a dense, thermally self-reinforcing composite hydrophobic layer with CTAB at the solid-oil interface; and establishment of a weak three-dimensional network in the continuous phase for uniform particle suspension. This work not only presents a high-performance and environmentally compatible additive but, more importantly, establishes a distinct molecular design paradigm focused on solid-phase wettability control and sag prevention for stabilizing ultra-low OWR drilling fluids.

KEYWORDS: Oil-based drilling fluid; ultra-low oil-to-water ratio; wetting agent; hyperbranched polymer; barite sag

1 Introduction

OBDFs are indispensable in demanding operations such as deepwater, ultra-deep, and extended-reach wells due to their superior lubricity, shale inhibition, and thermal stability. However, their high cost, limited temperature resistance, and susceptibility to contamination pose significant challenges during drilling operations [1–4]. To address these economic and environmental pressures, a key trend in OBDF development is the continuous reduction of the OWR [5–7]. As the OWR is reduced to ultra-low levels (e.g., below 70:30), the primary technical bottleneck shifts from conventional emulsion instability to an acute

and fundamentally different challenge: solid-phase control. Specifically, the catastrophic settling of barite—termed barite sag—becomes critically exacerbated. This phenomenon arises from two converging factors: the inherent hydrophilicity of barite particles, which resist dispersion in the oil phase, and the drastically diminished suspending capacity of the shrinking continuous oil phase. Barite sag leads to severe density stratification along the wellbore, posing direct risks to well control and drilling efficiency. Therefore, directly engineering the barite surface wettability represents a more targeted solution than relying solely on emulsion viscosity or interfacial film strength [8–12].

Current strategies to mitigate sag rely heavily on wetting agents. Current wetting agents for oil-based drilling fluids primarily include small-molecular surfactants and polymeric agents, with emerging research into nano-material-based and composite systems [13–17]. While conventional surfactant-based wetting agents are prone to weak adsorption and thermal desorption in demanding environments, polymeric agents offer a promising alternative. As reviewed elsewhere [18], hyperbranched polymers combine multi-functional topology with thermal robustness, making them attractive for demanding interfacial applications. They were reported to be applied in the separation of oil-in-water emulsion, membranes, thermal interface materials, biomedical, etc. [19–23]. Very recently, hyperbranched polymers have also been explored for flame-retardant composite applications [24]. Nevertheless, the deliberate design of hyperbranched polymers as high-performance wetting agents specifically targeting solid-phase control in ultra-low OWR OBDFs remains unexplored. Existing studies have primarily focused on hyperbranched emulsifiers for oil-water interface stabilization [25,26], which addresses a fundamentally different challenge. Even a very recent study on hyperbranched polymers for barite sag relied primarily on rheological and interfacial effects rather than deliberate solid-surface wettability engineering [27]. Existing studies on hyperbranched polymers for drilling fluids have primarily focused on their role as emulsifiers or demulsifiers at the oil–water interface. For example, Wang et al. [28] recently reported a hyperbranched polyamide emulsifier for stabilizing ultra-low OWR emulsions. While effective for interfacial stabilization, such an approach addresses the continuous phase and the emulsion structure rather than the surface properties of the solid weighting material. In contrast, the distinct requirements for solid-phase control—specifically, strong chemisorption onto barite surfaces and the formation of a stable, thermally robust oleophilic shell—demand a fundamentally different molecular design. Our HP-Wet is engineered precisely to meet these solid-specific requirements.

This paper presents the design, synthesis, and performance assessment of HP-Wet, with an emphasis on its unique solid-surface anchoring mechanism. Our strategy focuses on: (1) incorporating phosphonate groups for strong, specific chelation with barite surface ions, ensuring irreversible adsorption; (2) constructing a hyperbranched polyamide scaffold to provide multiple anchoring points and a bulky structure for effective steric hindrance; and (3) functionalizing with long alkyl chains to create a dense oleophilic shell. We systematically investigate the synergistic effect between HP-Wet and a cationic co-agent (CTAB), which further enhances the hydrophobic layer through electrostatic complexation. This work elucidates the multi-scale stabilization mechanism unique to solid-phase control, from molecular anchoring to macroscopic network formation, establishing a new paradigm for developing high-performance sag control additives and differentiating itself clearly from prior work on hyperbranched emulsifiers for interface stabilization.

2 Materials and Methods

2.1 Materials

The experimental reagents and instruments for the synthesis of HP-Wet and the formulation & testing of drilling fluids used in this work are listed in Tables 1 and 2.

Table 1: Experimental reagents.

Material	Purity/ Grade	Supplier
Polyether amine (D-230)	96.0%, M_w~2000	Shanghai Zeyye Biotechnology Co., Ltd.
Timellitic anhydride (TMA)	99.0%	Merck, Rahway, NJ, USA
Lauric Acid	99.0%	Hubei Baidu Chemical Co., Ltd.
p-Toluenesulfonic acid (PTSA)	98.0%	Aladdin, Shanghai, China
Calcium hydroxide	99.0%	Sinopharm Group, Shanghai, China
Phenylphosphonic Acid (PPA)	98.0%	Merck, Rahway, NJ, USA
Phosphoethanolamine (PEA)	98.0%	Aladdin, Shanghai, China
Stearyl glycidyl ether	98.0%	Aladdin, Shanghai, China
Tetrahydrofuran (THF)	99.9%	Merck, Rahway, NJ, USA
Cetyltrimethylammonium Bromide (CTAB)	99.0%	Aladdin, Shanghai, China
Commercial wetting agent (X-407)	70% wt.%	Jiangsu Hai'an Petrochemical Factory
Sorbitan monooleate (Span 80)	95%	Nanjing Reagent
Organobentonite	99.0%	Hefei Flora Intelligent Technology Co., Ltd.
Barite	95.0%	Tianjin Yandong Haotian Mineral Products Co., Ltd.

Table 2: Experimental instruments.

Instrument	Model	Manufacturer
Fourier-transform infrared (FTIR) spectrometer	Nicolet iN10	Thermo Fisher Scientific, Shanghai
Thermogravimetric analyzer (TGA)	STAReSW	Swiss Mettler Toledo Company
Gel permeation chromatography (GPC)	Agilent 1260 Infinity	Agilent Technologies, Inc., Santa Clara, CA, USA
Contact Angle Goniometer	CA100	Kunshan Beidou Precision Instruments Co., Ltd.
Spinning Drop Tensiometer	YP-ZL10	Shandong Jiuzhang Scientific Instrument Co., Ltd.
Six-speed viscometer	ZNN-D6	Changzhou Dedu Precision Instrument Co., Ltd.
High-temperature roller heating furnace	XGRL-4A	Huangdao Senweida Electromechanical Equipment Business Department
Electrical stability tester	DWY-2	Qingdao Haitongda Special Instrument Co., Ltd.
HTHP filtration tester	GGS71-B	Hengtaida Mechanical and Electrical Equipment Co., Ltd.
Laser Diffraction Particle Size Analyzer	Mastersizer 3000	Malvern Panalytical
^{1}H NMR spectrum	Avance III 400 MHz	Bruker

2.2 Synthesis of the HP-Wet

HP-Wet was synthesized through a deliberate two-step strategy comprising controlled polycondensation followed by targeted functionalization, designed to precisely engineer its molecular architecture. We first prepared an amine-terminated hyperbranched scaffold via melt polycondensation of trimellitic anhydride and polyether amine D-230. The key innovation lies in the subsequent two-step grafting: (i) phosphoethanolamine to introduce phosphonate anchors, and (ii) stearyl glycidyl ether to confer oleophilicity. To prevent gelation and target a specific molecular weight, the molar ratio of amine to anhydride groups (r) was systematically varied from 1.01 to 1.09 (see Table 3) while keeping the TMA mass constant at 10.00 g. Reactions were carried out at 140°C under a nitrogen atmosphere for 8–10 h. The prepolymer obtained at the optimal ratio (identified by GPC analysis) was subsequently functionalized. Based on its titrated amine value, phosphoethanolamine (1.20 equiv. per-NH_2) and stearyl glycidyl ether (1.00 equiv. Per-NH_2) were sequentially added at 90°C using p-toluenesulfonic acid as a catalyst, and the mixture was reacted for 6 h. The crude product was purified by dissolution in THF, double precipitation into cold diethyl ether, and drying under high vacuum at 60°C for 24 h, yielding the final polymer as a pale-yellow solid. This synthetic approach—employing amine-excess stoichiometry to generate a soluble hyperbranched scaffold, followed by grafting of phosphonate (for barite anchoring) and long alkyl chains (for oleophilicity)—ensures strong multi-point adsorption and effective steric stabilization, which together underpin the outstanding sag control performance of HP-Wet.

Table 3: Reagent amounts for HP-Wet synthesis under different molar ratios.

Molar Ratio	TMA (g)	D-230 (g)	Product Label
1:1.01	10.00	18.14	HP-Wet-1.01
1:1.03	10.00	18.50	HP-Wet-1.03
1:1.05	10.00	18.86	HP-Wet-1.05
1:1.07	10.00	19.23	HP-Wet-1.07
1:1.09	10.00	19.59	HP-Wet-1.09

2.3 Characterization of HP-Wet

We employed multiple techniques to characterize the synthesized HP-Wet: FTIR, TGA, ^{1}H NMR, and GPC. FTIR analysis was conducted on a Nicolet iN10 spectrometer (ATR mode) over the range of 4000–400 cm^{-1} at a resolution of 4 cm^{-1} (32 scans per spectrum). For thermal stability, a STAReSW TGA system was used under N_2 atmosphere, heating about 10 mg of sample from 30 to 650°C at 10°C/min. ^{1}H NMR spectra were acquired at 25°C on a Bruker Avance III 400 MHz instrument, with the sample dissolved in DMSO-d_6 (approx. 10 mg in 0.6 mL) and chemical shifts referenced to TMS (δ = 0 ppm). Molecular weight and its distribution were determined by GPC (Agilent 1260 Infinity, THF eluent at 1.0 mL/min, calibrated with narrow polystyrene standards).

2.4 Preparation and Formulation of OBDFs

To guide formulation development, initial screening tests targeted a balanced performance across emulsion stability, rheology, and fluid loss control at an OWR as low as 55:45. OBDFs with different OWRs were tested against each other. Table 4 shows the base recipe. Three fluid systems were compared: a CTAB-free base fluid; a version where the HP-Wet/CTAB pair was swapped for a commercial wetting agent; and a version containing the laboratory-synthesized HP-Wet/CTAB synergistic emulsifier.

Table 4: Composition and mixing order of the OBDF base formulation (OWR = 55:45).

Additive	Function	Amount	Step
White mineral oil	Base Oil	60 parts (by weight) in OWR	1
CTAB	Emulsifier	5.0 wt.% of oil phase	2
Organoclay	Viscosifier	2.8 vol.% of total	3
30% $CaCl_2$ Solution	Aqueous Phase	40 parts (by weight) in OWR	4
HP-Wet (or Commercial)	Wetting Agent	Varied (0.5–2.5 vol.%)	5
Calcium oxide	pH Control Agent	3.5% v/v of total fluid	5
Fluid Loss Reducer	Leak-Off Reducer	4.0% v/v of total fluid	6
Baryte	Density Control Agent	Sufficient to reach 1.8 g/cm^3	7

Note: wt.% abbreviates weight percentage; vol.% stands for volume percentage. The concentrations of the primary emulsifier, organoclay, and filtration loss additive were adjusted based on preliminary rheology and emulsion stability screening to achieve optimal performance for the current wetting agent study.

The mixing protocol strictly followed the additive order given in Table 4, which was designed to ensure stepwise dissolution and hydration while preventing any incompatibility among components. First, the base oil, emulsifier, and synergistic agent were combined under mechanical stirring at 10,000 rpm for 20 min. Organoclay was then incorporated and stirred for another 30 min. Next, the wetting agent and lime were added, with mixing continued at 8000 rpm for 10 min. The $CaCl_2$ brine was slowly introduced and the mixture was emulsified at 10,000 rpm for 45 min to form a stable invert emulsion. Thereafter, the fluid-loss reducer was blended in at 8000 rpm for 20 min. After all components were well dispersed, barite was gradually fed at 4000–6000 rpm until a density of 1.8 g/cm^3 was reached, followed by homogenization at 10,000 rpm for 30 min to obtain the base slurry. To simulate downhole thermal environments, each formulation was dynamically hot-rolled at 90°C, 120°C, 150°C, or 180°C for 16 h. After cooling and remixing, the samples were evaluated according to API 13B-2 [29].

2.5 Assessment of Drilling Fluid Properties

Each test described below was repeated three times. Data are presented as mean values with their standard deviations.

2.5.1 Rheological Property Measurements

Measured using a six-speed viscometer. Apparent viscosity (AV), plastic viscosity (PV), and yield point (YP) were calculated using the following standard Eqs. (1)–(3) [30].

$$AV = 0.5\varphi 600 \tag{1}$$

$$PV = \varphi 600 - \varphi 300 \tag{2}$$

$$YP = AV - PV \tag{3}$$

2.5.2 Electrical Stability Test

Electrical stability (ES) was measured with a DWY-2 device according to API 13B-2. After placing 50 mL of well-mixed drilling fluid into the test cup, the sample was heated to 55 ± 1°C in a water bath and held for 10 min, with light hand-stirring immediately before the test. A cylindrical electrode pair was inserted, and a linear voltage increase (150 V/s) was applied. The maximum voltage reached before a sharp current drop (indicating emulsion breakdown) was recorded as the ES [31].

2.5.3 HTHP FL Test

HTHP filtration loss was assessed according to the literature [32]. Briefly, OBDFs with varying HP-Wet dosages were stirred at 10,000 rpm for 20 min, then hot-rolled for 16 h at temperatures of 90°C, 120°C, 150°C, and 180°C. Subsequently, the HTHP FL was determined with a standard filtration tester at the same aging temperature under 3.5 MPa.

2.5.4 Settlement Stability Test

The sag factor (SF), a quantitative index of sedimentation stability, was determined via a static sedimentation method commonly used in field operations [33]. In this test, each sample was hot-rolled for 16 h at a given temperature, then statically aged at room temperature for 24 h. The densities of the upper (ρ_{top}) and lower (ρ_{bottom}) layers were measured with a drilling fluid densimeter, and the SF was calculated as follows [34]:

$$SF = \frac{\rho_{bottom}}{\rho_{bottom} + \rho_{top}} \tag{4}$$

Values of SF above 0.52 indicate severe barite settling within the fluid, while an SF equal to 0.50 reflects ideal sag resistance (no detectable settlement). The influence of inclination was further investigated by conducting additional tests at 0°, 45°, and 90° (vertical to horizontal). These results are summarized in Section 3.3.3.

2.5.5 Contact Angle Measurement and Wettability Evaluation

The efficiency of the wetting agents in modifying barite surface wettability was quantitatively assessed by static water contact angle measurements using an optical contact angle goniometer (CA100, Kunshan Beidou Precision Instruments Co., Ltd.). Barite pellets were prepared by compressing pure API-grade barite powder under a uniaxial pressure of 10 MPa for 3 min to ensure a smooth and consistent surface. Each pellet was then fully immersed in a 1.5 vol.% solution of the wetting agent (HP-Wet or commercial reference) in white oil for 24 h at ambient temperature to achieve adsorption equilibrium, after which it was retrieved, rinsed with fresh oil, and dried. A 3 μL droplet of deionized water was dispensed onto the treated pellet surface under controlled ambient conditions (25 ± 1°C, 50 ± 5% RH). The static contact angle was automatically determined by the instrument's software using the sessile drop fitting method after a 5-s stabilization period. For statistical reliability, at least three independent measurements were taken on different surface locations per sample, with the mean value and standard deviation reported.

2.5.6 Biological Toxicity Measurements

We assessed the environmental compatibility of the OBDF using a luminescent bacteria bioassay, a well-established method for rapid ecotoxicological screening in the drilling fluid industry [35]. The half-maximal effective concentration (EC_{50}) was derived following standard protocols [36]. Although full-spectrum, multi-species toxicity tests would offer broader ecological insight, the luminescent bacteria test provides a practical and standardized metric for initial environmental risk assessment [37].

2.6 Analysis of Interfacial and Colloidal Properties

To gain mechanistic insight into emulsion stabilization and barite sag prevention, additional measurements of interfacial and microstructural features were conducted.

2.6.1 Interfacial Tension Measurement

The synergy between HP-Wet and CTAB was assessed via equilibrium interfacial tension (IFT) measurements at the oil–brine interface (white oil vs. 30 wt.% $CaCl_2$). A spinning drop tensiometer was used at 25°C. IFT readings were taken for three systems: HP-Wet only, CTAB only, and their 55:45 mixture, thereby revealing the extent of molecular cooperativity.

2.6.2 Emulsion Droplet Size Analysis

Laser diffraction was used to characterize the invert emulsion microstructure, which reflects the performance of the emulsifier system. To avoid disrupting the original droplet structure, samples were mildly diluted with white oil and analyzed promptly without high-shear mixing. The volume-weighted median diameter (D50) and polydispersity index (PDI) were adopted as metrics for emulsion homogeneity and stability.

2.6.3 Zeta Potential and Aggregate Size of Emulsifier Dispersions

Zeta potential and aggregation behavior of HP-Wet and HP-Wet/CTAB in the continuous oil phase were measured as indicators of interfacial charge and heat-induced conformational changes. Sample preparation involved dilution in white oil, ultrasonication to ensure uniform dispersion, and centrifugation to remove large particulates (e.g., barite). The supernatant was then analyzed for its zeta potential and hydrodynamic diameter, aiming to reveal any thermally triggered self-reinforcement effect at the interface.

2.7 HP-Wet Adsorption Measurements

Zeta potential of barite after HP-Wet adsorption was measured in a background electrolyte (0.1 M NaCl, 0.01 M Na_2SO_4, pH 9.0). HP-Wet concentrations: 0, 0.1, 0.5, 1.0, 2.0 wt.%. Barite (0.1 g) was mixed with 10 mL of each solution, shaken at 200 rpm for 30 min at 25°C. After brief sedimentation, the supernatant was analyzed using a zeta potential analyzer (three measurements per sample, three replicates per concentration).

3 Results and Discussion

3.1 Characterization

As shown in Fig. 1, the FTIR spectrum confirms the key structural features essential to the HP-Wet. The broad absorption at 3270 cm^{-1} and the strong band at 1709 cm^{-1} are characteristic of the poly(amic acid) intermediate, resulting from the condensation of TMA and D-230. These indicate the presence of hydrogen-bonded carboxylic acid O-H/N-H and carbonyl (C=O) groups, respectively, forming the polymer backbone. The peak at 1535 cm^{-1} (amide II) further confirms amide linkage formation. Critically, the intense peak at 1235 cm^{-1} is definitive evidence for the P=O stretching vibration of the incorporated phenylphosphonic acid (PPA), which is the key anchoring group for barite. Its associated P-O-C linkage is suggested by the absorption at 1043 cm^{-1}. The presence of the flexible polyether chain from D-230 is verified by the C-O-C stretch at 1143 cm^{-1}, while the strong aliphatic C-H stretches at 2924 and 2854 cm^{-1}, along with the aromatic C-H out-of-plane bend at 864 cm^{-1}, confirm the successful grafting of the long alkyl chain (from lauric acid) and the preservation of the aromatic rings from TMA/PPA. Therefore, the FTIR spectrum is fully consistent with the structure of HP-Wet, displaying all the diagnostic peaks for the hyperbranched poly(amic acid) scaffold, the oleophilic alkyl shell, and the phosphonate-based anchoring functionality.

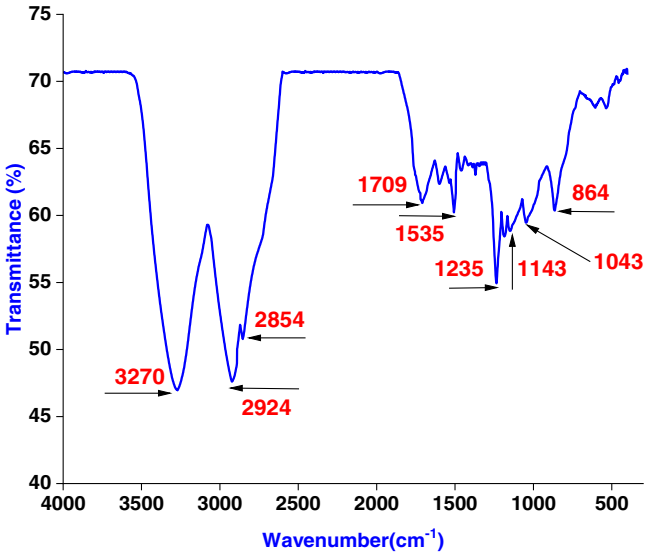

Figure 1: FTIR spectrum of HP-Wet.

Fig. 2 displays the ^{1}H NMR spectrum of HP-Wet, confirming the structural features. The signal at δ 0.898 and the intense peak at δ 1.274 are attributed to the terminal methyl and the long-chain methylene groups of the stearyl chains, respectively. The resonance at δ 3.056 corresponds to the -CH_2-NH- of the grafted phosphoethanolamine, while the broad signal at δ 3.689 arises from overlapping -O-CH_2- units of the polyether backbone, and the stearyl glycidyl ether. The PEA -O-CH_2-P protons appear as two distinct signals at δ 4.041 and 4.159, likely due to diastereotopic environments or different branching sites within the hyperbranched architecture. The peak at δ 7.283 is due to the $CDCl_3$ solvent; aromatic protons from the TMA-derived benzene ring are expected at δ 7.5–8.5 but are likely obscured by the solvent signal. The absence of any signal above δ 10 confirms the lack of free carboxylic or phosphonic acid groups, consistent with the successful amine-excess polycondensation and the intact phosphate ester structure.

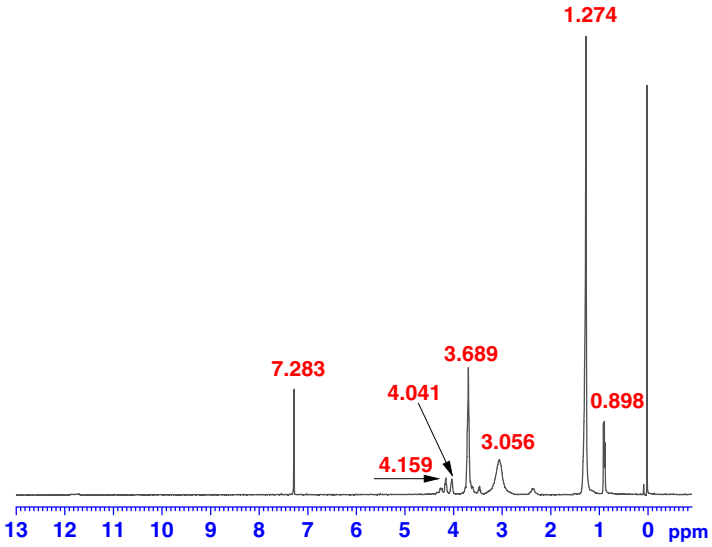

Figure 2: ^{1}H NMR of HP-Wet.

As illustrated in Fig. 3, the thermal decomposition of HP-Wet presents a characteristic profile when examined at three defining temperature points. The initial mass loss is minimal, reaching only 3.39% at 200°C, corresponding to the evaporation of residual moisture and trace volatile [38]. A second, more substantial decomposition stage is observed up to 320°C, with the cumulative mass loss reaching 13.74%. This stage corresponds to the breakdown of peripheral functional groups and less stable segments within the hyperbranched architecture. The most significant degradation occurs between 320°C and 500°C, where a rapid mass loss of 65.01% takes place, attributable to extensive scission of the polymer's primary backbone. This distinct three-stage profile—characterized by initial thermal stability, followed by moderate mid-temperature decomposition and a dominant high-temperature breakdown—directly stems from the material's unique three-dimensional hyperbranched structure. The compact molecular topology, combined with the extensive hydrogen-bonding network formed by amide groups, collectively restricts chain mobility. As a result, the release of volatile decomposition products is delayed and occurs in a staged manner. This inherent thermal resilience, characterized by controlled degradation rather than sudden failure, underpins the suitability of HP-Wet for application in demanding high-temperature environments such as ultra-low oil-to-water ratio drilling fluids.

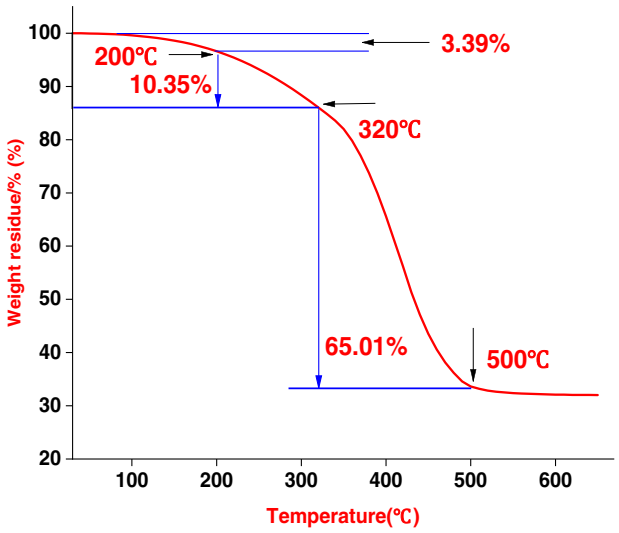

Figure 3: TGA curve of the synthesized HP-Wet.

GPC analysis elucidated the influence of the monomer molar ratio on the molecular architecture of the HP-Wet series (Table 5). As the amine proportion increased from 1:1.01 to 1:1.09, the molecular weight distribution first narrowed. HP-Wet-1.05 (synthesized at a 1:1.05 molar ratio) exhibited a well-balanced combination of moderate molecular weight (M_w = 31,021 g/mol) and the lowest PDI = 1.96) among the series. This profile is characteristic of a well-defined hyperbranched topology, which is hypothesized to facilitate effective diffusion and multi-point anchoring on barite surfaces. Therefore, HP-Wet-1.05 was selected for all subsequent performance evaluations. The variation in molecular weight and distribution across different monomer ratios stems directly from controlling the stoichiometric imbalance between the amine (NH_2) and anhydride groups, which dictates the growth and termination pathways in the hyperbranched polycondensation. When the amine is slightly in excess (e.g., r = 1.01–1.07), it acts as a controlled chain-terminating agent, preventing gelation by consuming all anhydride groups and allowing the formation of well-defined, high-molecular-weight hyperbranched structures with moderate PDI—optimal for multi-point anchoring. However, as the amine excess becomes too high (e.g., r = 1.09), excessive chain termination

dominates, prematurely capping growing chains and yielding lower-molecular-weight oligomers that lack the robust, persistent adsorption layer required for effective sag control.

Table 5: The molecular weight of the HP-Wet series polymers.

Sample	M_n	M_w	PDI (M_w/M_n)
HP-Wet-1.01	8462	19,328	2.28
HP-Wet-1.03	12,255	25,954	2.12
HP-Wet-1.05	15,818	31,021	1.96
HP-Wet-1.07	13,596	28,453	2.09
HP-Wet-1.09	9958	22,995	2.31

Note: M_n: number-average molecular weight; M_w: weight-average molecular weight; M_z: z-average molecular weight; PDI: polydispersity index. The HP-Wet-1.05 sample exhibits an optimal balance of moderate molecular weight and the lowest PDI, which is hypothesized to be most effective for barite surface modification and sag control.

3.2 Interaction between HP-Wet and Barite Surface

To verify the anchoring mechanism of HP-Wet on barite, zeta potential measurements were conducted on barite particles treated with varying HP-Wet concentrations. As shown in Fig. 4, pristine barite exhibited a negative zeta potential of –28.5 ± 1.0 mV. Upon addition of HP-Wet, the zeta potential progressively increased with concentration: to –19.9 ± 0.8 mV at 0.5 wt.%, –12.1 ± 0.8 mV at 1.0 wt.%, –7.5 ± 0.7 mV at 1.5 wt.%, and –2.6 ± 0.7 mV at 2.0 wt.%, approaching a plateau beyond 1.0 wt.%. This concentration-dependent charge neutralization provides direct evidence for HP-Wet adsorption, attributed to inner-sphere coordination of phosphonate groups ($–PO_3^{2–}$) with surface Ba^{2+} sites, consistent with literature on phosphonate adsorption on alkaline earth minerals. The results validate the proposed anchoring mechanism.

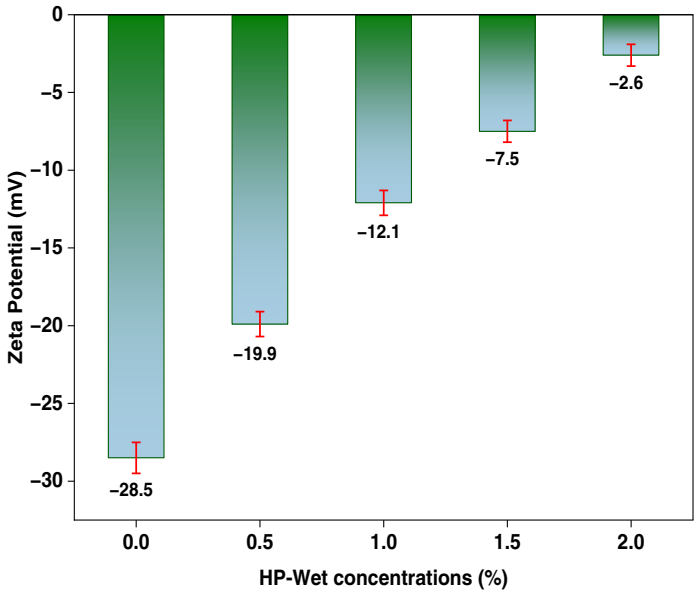

Figure 4: Zeta potential of barite particles as a function of HP-Wet concentration.

3.3 Optimization of Synthetic Formulation

3.3.1 Effect of HP-Wet Dosage on Wettability and Sedimentation Stability

The primary function of a wetting agent is to render solid particles oleophilic. We first quantified the efficacy of HP-Wet by measuring the static water contact angle on treated barite surfaces (Fig. 5, Table 6). Untreated barite was highly hydrophilic (21.9°). The contact angle increased dramatically with HP-Wet dosage, plateauing at approximately 117° at 2.0 vol.%, indicating successful and complete wettability reversal. This visual transformation (Fig. 5a–f) provides direct evidence of a dense oleophilic layer formed on barite. Correspondingly, the SF of the OBDF showed a clear minimum at this optimal dosage (0.504). The non-monotonic trend in SF suggests that while insufficient HP-Wet leads to poor coverage and sag, excess amounts may slightly perturb the fluid's colloidal structure. The concurrent increase in YP with dosage supports the formation of a stronger particle network. Therefore, 2.0 vol.% was identified as the optimal dosage, fundamentally solving the wettability issue as a prerequisite for sag control.

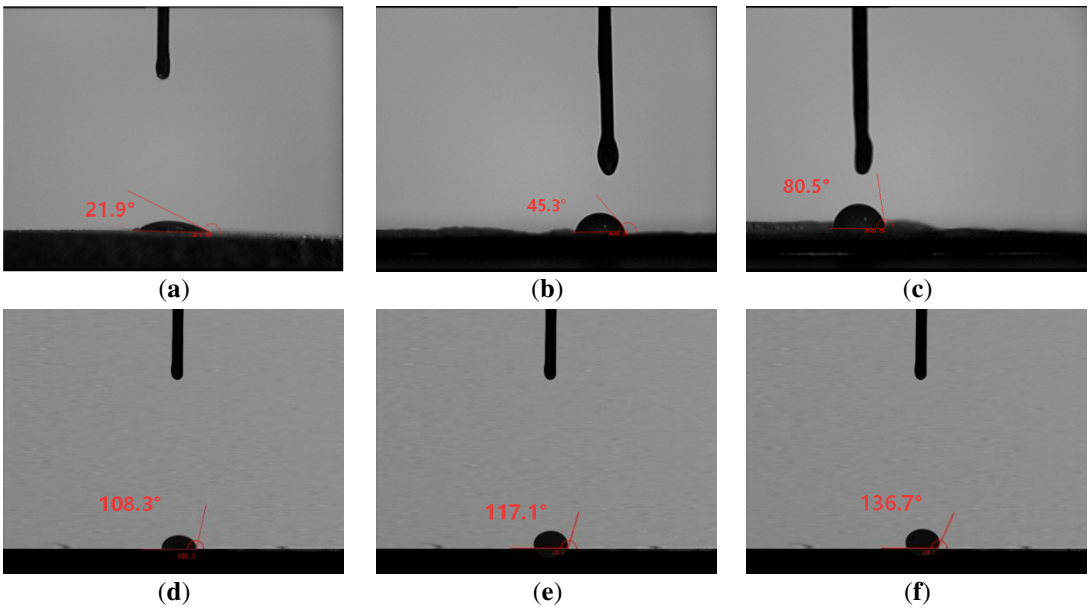

Figure 5: Static water contact angle images on barite surfaces treated with different dosages of HP-Wet: (**a**) 0 vol.%, (**b**) 0.5 vol.%, (**c**) 1.0 vol.%, (**d**) 1.5 vol.%, (**e**) 2.0 vol.%, (**f**) 2.5 vol.%.

Table 6: Optimization of HP-Wet dosage and its effect on wettability.

Wetting Agent Dosage (vol.%)	Contact Angle (°)	SF
0	21.9 ± 0.5	0.519
0.5	45.3 ± 1.2	0.514
1.0	80.5 ± 1.7	0.511
1.5	108.3 ± 2.1	0.509
2.0	117.1 ± 2.4	0.504
2.5	136.7 ± 3.5	0.513

3.3.2 Optimization of the HP-Wet to CTAB Ratio

Table 7 presents the optimization of the molar ratio between the HP-Wet and the CTAB. The data clearly identifies a 55:45 (HP-Wet:CTAB) ratio as optimal, delivering the best overall performance. This formulation achieves the highest ES (1168 V), indicating superior emulsion stability, alongside the lowest HTHP FL (2.2 mL) and SF (0.505), signifying excellent filtration control and barite suspension. The balanced rheology (PV = 32 mPa·s, YP = 9.2 Pa) further supports effective fluid structuring. Performance declines when deviating from this ratio, whether towards pure HP-Wet (100:0) or pure CTAB (0:100). This non-monotonic trend strongly indicates a synergistic effect between HP-Wet and CTAB. The hyperbranched architecture of HP-Wet likely provides multi-point anchoring and a structural scaffold, while CTAB enhances interfacial activity. Together at the 55:45 ratio, they form a denser, more cohesive, and thermally robust composite interfacial film, which is the foundation for the enhanced stability observed in subsequent ultra-low OWR tests.

Table 7: Optimization of the HP-Wet-to-CTAB molar ratio (OWR = 80:20).

HP-Wet:CTAB	PV/mPa·s	YP/Pa	ES/V	HTHP FL/mL	SF
100:0	22	3.8	728	8.1	0.529
70:30	27	6.5	926	4.1	0.517
55:45	32	9.2	1168	2.2	0.505
30:70	36	5.2	592	5.1	0.527
0:100	19	2.3	435	9.4	0.539

3.3.3 Optimization of Oil-to-Water Ratio

Table 8 details the optimization of the OWR for the system containing the optimal HP-Wet:CTAB (55:45) blend. The results reveal a critical trade-off: increasing the water phase (lowering the OWR) improves rheological structure and filtration control but challenges emulsion stability. As the OWR decreases from 90:10 to 55:45, the YP increases significantly from 3.8 to 13.8 Pa, enhancing cuttings transport and sag resistance (SF improves to 0.504). Concurrently, HTHP FL reaches a minimum of 1.7 mL at 55:45. However, the ES gradually decreases with more water, as the emulsifier system must stabilize a larger interfacial area. Crucially, at the 55:45 OWR, the system maintains an outstanding balance—ES remains high at 1156 V, well above the 800 V field requirement, while achieving optimal sag control and filtration. The 50:50 ratio represents the operational limit, where the interfacial film is overstretched, causing a sharp drop in electrical stability (to 705 V) and a rebound in the SF. Therefore, 55:45 is established as the optimal OWR, enabling the formulation of a high-performance, cost-effective, and environmentally favorable ultra-low-oil-phase drilling fluid.

Table 8: Optimization of the OWR (HP-Wet:CTAB = 55:45).

Oil-to-Water Ratio	PV/mPa·s	YP/Pa	ES/V	HTHP FL/mL	SF
90:10	25	3.8	1538	4.6	0.526
80:20	30	5.9	1395	3.5	0.517
70:30	41	9.5	1252	2.1	0.512
55:45	48	13.8	1156	1.7	0.504
50:50	65	18.5	705	2.6	0.535

3.3.4 Synergistic Specificity: Performance Comparison with a Model Nonionic Emulsifier

To critically evaluate the uniqueness of the synergy between HP-Wet and CTAB, a control formulation was prepared by replacing CTAB with Span 80, a widely used, oil-soluble, and biodegradable nonionic emulsifier. This comparison aims to determine whether the exceptional performance of the HP-Wet/CTAB system is a general outcome of HP-Wet pairing with any effective emulsifier, or a specific result of its chemical partnership with CTAB. The HP-Wet/Span 80 blend was maintained at the same optimal weight ratio (55:45) and OWR (55:45) as the HP-Wet/CTAB system for a direct and fair comparison. The key performance metrics of both systems after hot-rolling aging at 180°C are summarized in Table 9.

Table 9: Performance comparison of HP-Wet synergistic systems with different emulsifiers after hot-rolling at 180°C for 16 h.

System	PV (mPa·s)	YP (Pa)	ES (V)	HTHP FL (mL)	SF
HP-Wet/CTAB (55:45)	44	10.5	1069	1.9	0.509
HP-Wet/Span 80 (55:45)	36	7.5	825	2.8	0.518

As clearly shown in Table 9, the HP-Wet/Span 80 system exhibited significantly inferior performance. Crucially, its ES (825 V) was substantially lower than that of the HP-Wet/CTAB system (1069 V), and its SF (0.521) deteriorated to near the warning threshold. This divergence stems from a fundamental difference in interfacial molecular synergy. The cationic CTAB engages in strong electrostatic/polar interactions with the phosphonate groups of HP-Wet, enabling the formation of a dense, cohesive composite film responsible for the high ES and superior suspension (SF = 0.506). In contrast, the nonionic Span 80 lacks the specific functionality to form similarly strong associative bonds with HP-Wet. Consequently, the resulting weaker mixed film leads to the observed deficits in stability and control. This confirms that the exceptional performance arises from a specific molecular partnership, not a generic emulsifier effect.

3.4 Comprehensive Performance Evaluation of the Optimized OBDF System

This section presents a comprehensive evaluation of the OBDF system's performance, focusing on its ability to solve the primary challenge of barite sag under ultra-low OWR (55:45) conditions. Three systems were compared: (1) a Base Fluid without a dedicated wetting agent, (2) a Base Fluid with the commercial wetting agent X-407, and (3) a Base Fluid with the synthesized HP-Wet. All systems were subjected to hot-rolling aging at 90°C, 120°C, 150°C, and 180°C for 16 h. The evaluation prioritizes sag stability as the central performance metric, supported by analysis of its underlying causes and beneficial consequences for other fluid properties. All tests were conducted in triplicate. The results are reported in the text and tables as the mean ± standard deviation, with the corresponding error bars.

3.4.1 High-Temperature Tolerance and Overall Performance: A Sag-Focused Assessment

As summarized in Table 10, the OBDF formulated with the synthesized HP-Wet exhibited comprehensively superior performance over both the base fluid and the fluid containing X-407 after severe aging at 180°C. The most critical achievement is its exceptional sag control, the HP-Wet system achieved an outstanding SF of 0.511, well below the 0.52 warning threshold and significantly lower than the base fluid (0.535). This value is not only well below the 0.52 warning threshold but also significantly lower than that of the base fluid (0.535) and the commercial X-407 formulation (0.517). This outstanding performance is the direct result of HP-Wet's proven efficacy in fundamentally reversing barite wettability (contact angle > 117°), as established in Section 3.2. The system's other enhanced properties are understood as synergistic outcomes

and enablers of this core sag control function: Enhanced Rheology: The highest PV and a markedly increased YP (9.9 Pa) indicate the formation of a stronger internal gel structure, which is the macroscopic manifestation of the particle suspension network that resists settlement. Robust Emulsion Stability: The high electrical stability (ES, 1128 V) suggests that the HP-Wet/CTAB system does not compromise, and may actively reinforce, the oil-water interface, providing a stable continuous phase essential for particle suspension. Superior Filtration Control: The lowest HTHP FL (1.9 mL) is a beneficial consequence of improved barite dispersion and packing, enabled by effective surface modification. Thus, the performance profile confirms that the HP-Wet/CTAB system directly and effectively addresses the core challenge of solid-phase stability in ultra-low-OWR OBDFs.

Table 10: Comprehensive performance comparison of different OBDF systems after hot-rolling at 180°C for 16 h.

System	PV (mPa·s)	YP (Pa)	ES (V)	HTHP FL (mL)	SF
Base Formulation	29	6.1	594	3.8	0.535
Base Formulation + X-407	32	7.9	915	2.6	0.517
Base Formulation + HP-Wet	38	9.9	1128	1.9	0.511

Note: X-407 is a 70 wt.% solution; HP-Wet is 100% active. Concentrations are vol.% of as-received materials.

3.4.2 Emulsification Stability

Emulsion stability is paramount for the overall performance and safety of OBDFs. It was evaluated by the ES, with a higher value indicating greater stability. A minimum ES of 800 V is typically required for field applications [39]. As shown in Fig. 6, the ES of all three systems declined with increasing aging temperature, reflecting progressive thermal degradation. The Base Formulation was the most vulnerable, with its ES falling below the critical 800 V threshold after aging at 180°C, Remarkably, the HP-Wet system not only maintained sufficient emulsion stability (ES > 1000 V) but also exhibited a significant rebound in ES at 180°C. This anomaly suggests that the HP-Wet/CTAB complex may actively reinforce the oil-water interface under thermal stress, a mechanism investigated in Section 3.4.2. This synergistic enhancement of interfacial stability, while not the main target, provides a more reliable continuous phase for the suspended barite particles, thereby indirectly supporting superior sag control.

3.4.3 Sag Stability under High-Density and Deviated Wellbore Conditions: The Definitive Performance Benchmark

Evaluating sag stability under simultaneous thermal stress and wellbore inclination represents the most demanding operational condition. Fig. 7a shows that across all aging temperatures, the HP-Wet-based fluid consistently gave the lowest SF. The superior performance becomes even more evident under deviated wellbore geometries (Fig. 7b). After 16 h of dynamic aging at 180°C, the HP-Wet system kept SF values below the 0.52 threshold regardless of the inclination angle (0°, 45°, or 90°), indicating excellent isotropic and angle-independent suspension capability. In contrast, the two comparative formulations failed at 45° and/or 90° inclinations. This remarkable outcome stems directly from a unique three-dimensional network that the HP-Wet/CTAB complex builds within the continuous oil phase. Such a network imparts uniform gel strength, effectively suspending the surface-modified barite particles irrespective of hole orientation—a microstructural advantage that conventional additives cannot offer.

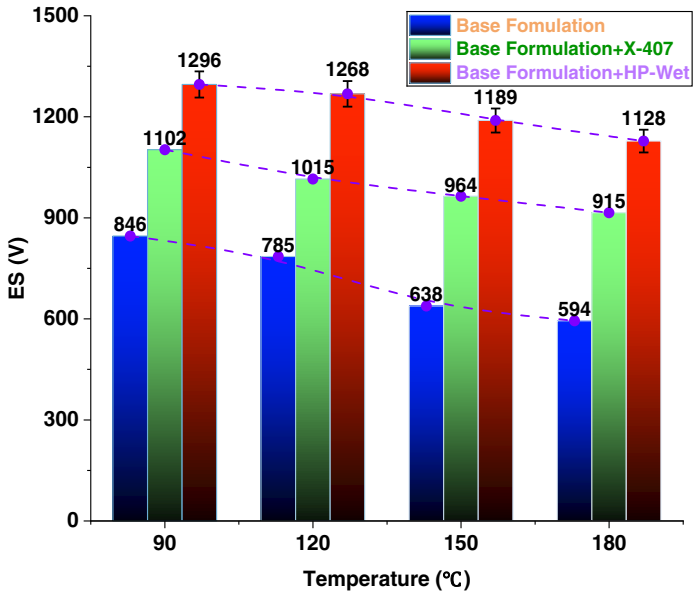

Figure 6: Electrical stability of HP-Wet-containing OBDFs after aging at 90°C–180°C, compared with base fluid and commercial X-407.

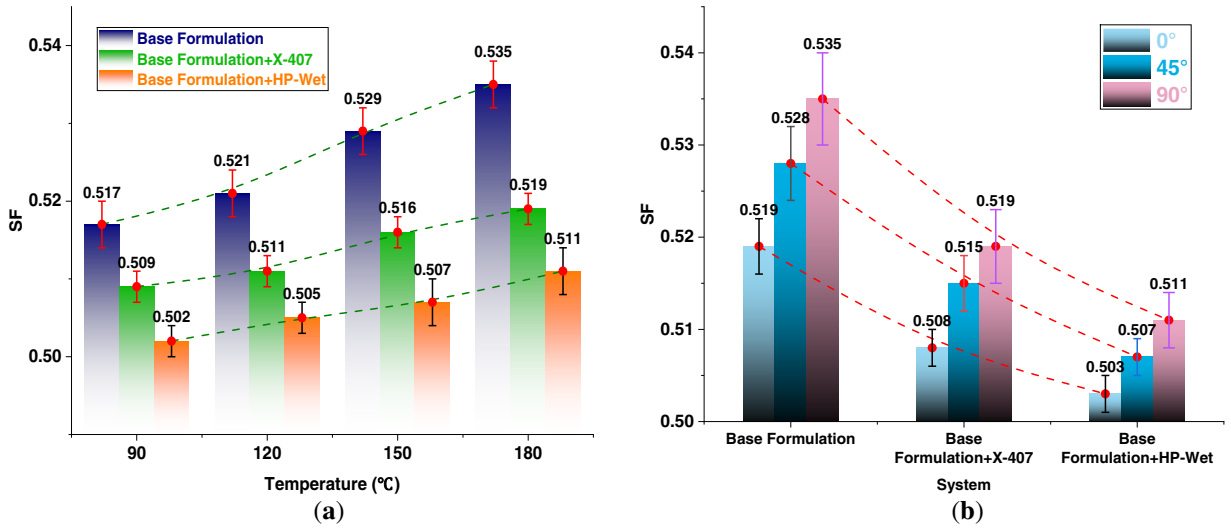

Figure 7: (**a**) Variation of SF with thermal aging temperature for different OBDF systems after hot-rolling at 180°C. (**b**) SF of different OBDF systems under various static inclination angles after hot-rolling at 180°C.

3.4.4 HTHP FL

As illustrated in Fig. 8, the HP-Wet system delivered the lowest HTHP fluid loss across the tested temperature range. This superior filtration control is a direct benefit of the effective barite surface modification achieved by HP-Wet. By rendering barite oleophilic and preventing particle aggregation, HP-Wet enables the generation of a filter cake characterized by minimal thickness, reduced permeability, and optimized solid particle compaction. Consequently, the excellent filtration control is an integrated outcome of the successful solid-phase management strategy, further validating the comprehensive effectiveness of the HP-Wet system.

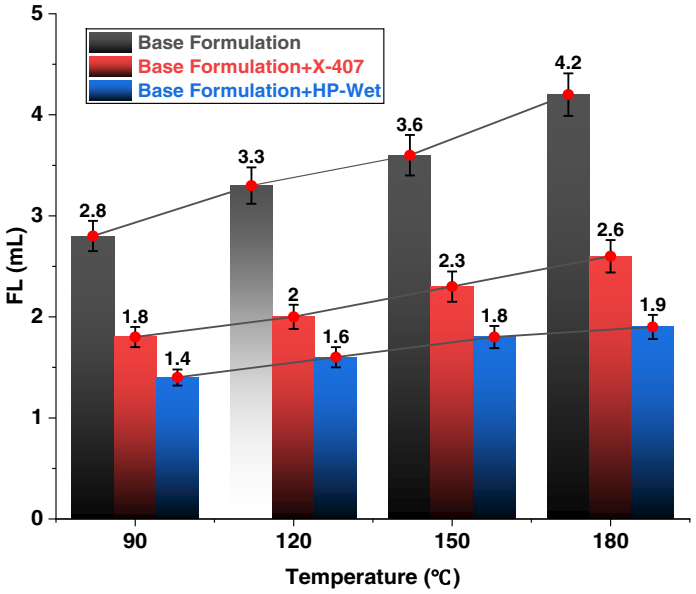

Figure 8: Variation of HTHP FL with thermal aging temperature for different OBDF systems after hot-rolling at 180°C.

3.4.5 Biological Toxicity Tests

We determined the EC_{50} values of the three OBDF formulations using the luminescent bacteria method (industry standard Q/SY 111–2007) [40], As summarized in Table 11, the EC_{50} values were 26,570 mg/L for the Base Formulation, 31,580 mg/L for the commercial X-407 formulation, and 37,600 mg/L for the HP-Wet-optimized formulation. Following the established toxicity classification [41], an EC_{50} > 25,000 mg/L indicates that the fluid is non-toxic, while a value exceeding 30,000 mg/L meets the permissible discharge criterion. Consequently, both the X-407 and HP-Wet formulations are non-toxic. Among them, the HP-Wet system gave the highest EC_{50}, indicating its best environmental compatibility.

Table 11: Ecotoxicity results for the three OBDF formulations.

Formulation	EC_{50} (mg/L)	Toxicity Classification
Base Formulation	26,570	Non-toxic
Base Formulation + X-407	31,580	Non-toxic
Base Formulation + HP-Wet	37,600	Non-toxic

3.5 Multi-Scale Mechanism of Solid-Phase Wettability Control

Unlike emulsifier-based systems that stabilize the oil–water interface, our mechanism focuses on the barite–oil interface. The superior ability of the HP-Wet-optimized OBDF system to resist barite sag is realized by a multi-scale synergistic approach that specifically targets solid-phase management. This mechanism, conceptually summarized in Fig. 9, operates across molecular, interfacial (solid-oil), and bulk-phase scales, distinctly different from the interface-dominated stabilization in emulsifier systems.

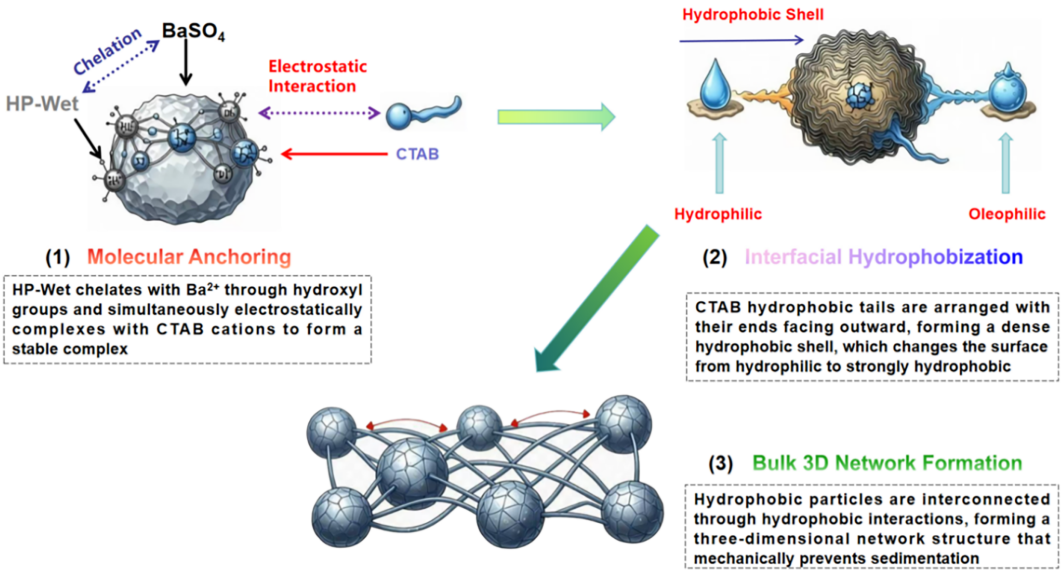

Figure 9: Schematic illustration of the multi-scale mechanism for barite sag control enabled by the HP-Wet/CTAB synergistic system **(1)** molecular scale: phosphonate groups chelate with Ba^{2+} on barite surface, and CTAB electrostatically locks the layer. **(2)** Particle scale: a thermally self-reinforcing hydrophobic sheath forms on each barite particle. **(3)** Bulk scale: a weak 3D network suspends the modified barite particles uniformly, providing angle-independent sag resistance.

3.5.1 Molecular-Scale Anchoring on Barite: Phosphonate–Barium Chelation and Electrostatic Locking

The mechanism is initiated at the molecular level by the strong, multi-point coordination between the phosphonate groups of HP-Wet and barium ions on the barite surface. This specific chelation ensures irreversible primary adsorption. The cationic CTAB then electrostatically complexes with the cationic sites of the adsorbed HP-Wet layer, acting as a secondary "electrostatic lock" that significantly enhances the adsorption layer's thermal stability. Furthermore, the long alkyl chains of both components intertwine via hydrophobic interactions, collaboratively building a dense and robust oleophilic shell. This combined molecular action is directly responsible for the complete and durable wettability reversal (contact angle > 117°).

3.5.2 Formation of a Thermally Self-Reinforcing Hydrophobic Shell on Barite Particles

On each barite particle surface, the HP-Wet/CTAB complex assembles into a dense, thermally self-reinforcing hydrophobic sheath. This is not a free-standing oil-water interfacial film; rather, it is a directly adsorbed layer that renders the barite surface highly oleophilic (contact angle > 117°). This is corroborated by IFT measurements, which reveal a significantly lower IFT for their synergistic mixture compared to either component alone (Table 12). Notably, this composite architecture demonstrates a unique thermally triggered self-reinforcement behavior. As shown in Figs. 10–12, HP-Wet/CTAB layer on barite undergoes a thermally induced rearrangement, leading to a more compact and ordered hydrophobic shell. This is supported by the increased absolute zeta potential (from −34.2 to −37.1 mV) and the reduced hydrodynamic diameter of the emulsifier aggregates, indicating densification. This *in-situ* thermal annealing effect is distinct from the behavior of conventional emulsifiers, which typically suffer from desorption or coalescence under heat [42,43], resulting in a thinner, denser, and mechanically stronger film [44]. This *in situ* interfacial consolidation under thermal stress provides a plausible explanation for the system's retained high electrical stability (ES > 1000 V) even under the severe conditions of an ultra-low OWR of 55:45, and is further consistent with supported by the finer and more uniform emulsion droplet size distribution observed

after aging (Table 13). The proposed thermally induced reinforcement thus remains a hypothesis requiring direct validation. In sharp contrast, the conventional X-407/CTAB system suffered from severe droplet coalescence after identical aging, with the D50 increasing by over 35% and the distribution broadening significantly (Table 13). This stark difference unequivocally highlights the superior thermal resilience and unique interfacial self-reinforcement capability of the HP-Wet/CTAB complex.

Table 12: IFT for different emulsifier systems.

Emulsifier System	IFT (mN/m)
Blank (Oil/Brine)	21.2 ± 0.3
X-407	12.4 ± 0.2
HP-Wet only	5.6 ± 0.1
CTAB only	7.9 ± 0.2
HP-Wet/CTAB (55:45)	2.5 ± 0.1
X-407/CTAB	4.7 ± 0.2

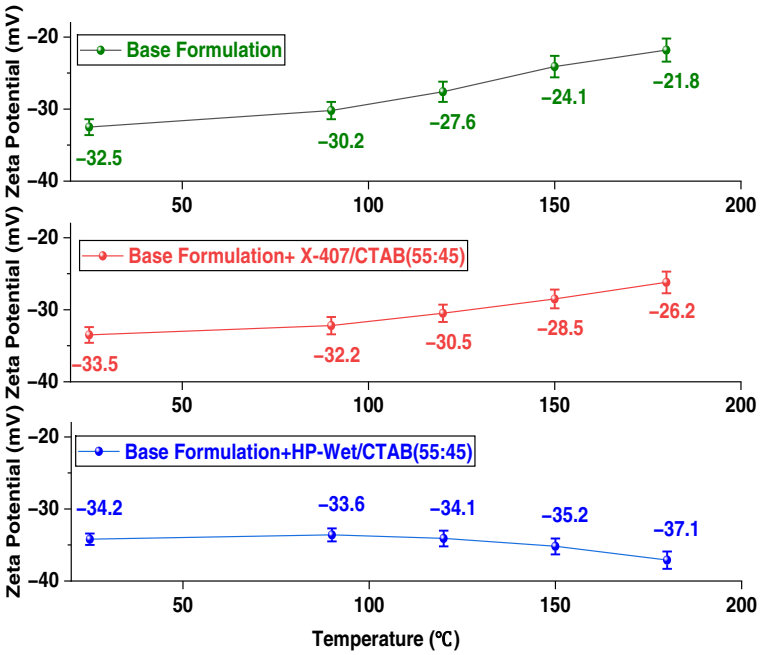

Figure 10: Zeta potential of different drilling fluid systems at varying temperatures.

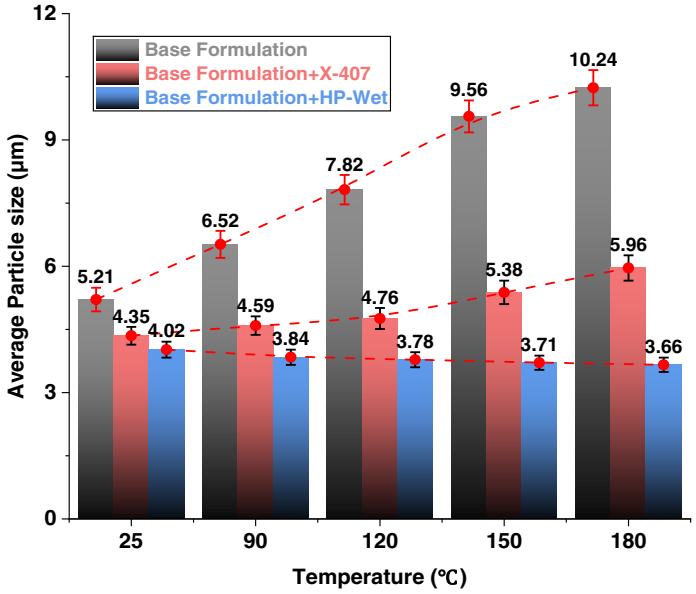

Figure 11: Particle size of different drilling fluid systems at varying temperatures.

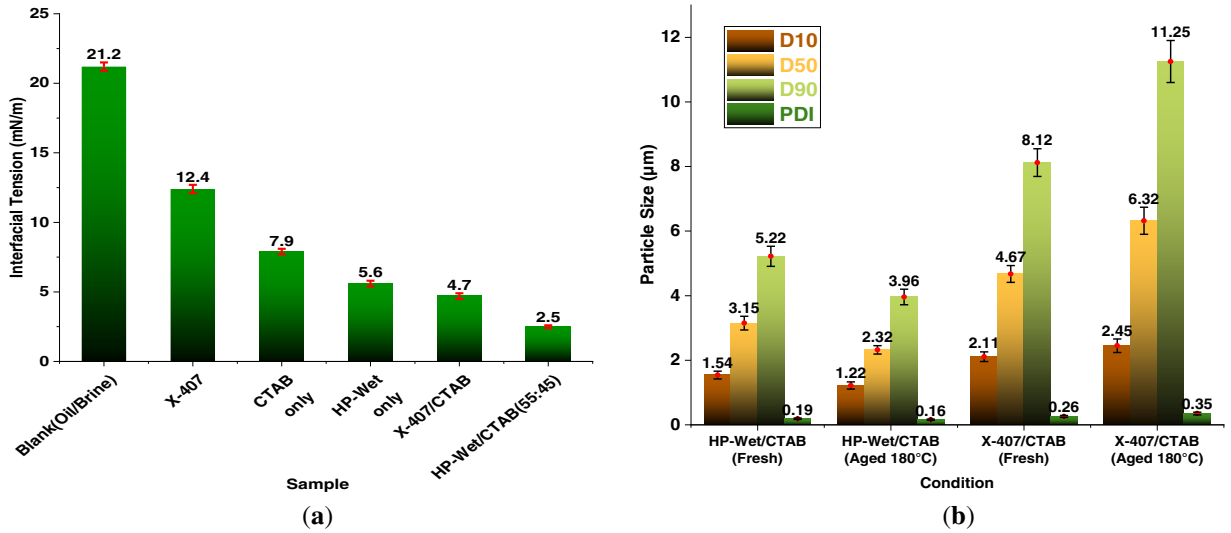

Figure 12: (**a**) IFT between white oil and 30% $CaCl_2$ solution for different emulsifier systems. (**b**) Emulsion droplet size.

Table 13: Emulsion droplet size for different emulsifier systems.

Condition	D_{10} (μm)	D_{50} (μm)	D_{90} (μm)	PDI
HP-Wet/CTAB (Fresh)	1.54 ± 0.12	3.15 ± 0.21	5.22 ± 0.31	0.19 ± 0.02
HP-Wet/CTAB (Aged 180°C)	1.22 ± 0.11	2.32 ± 0.13	3.96 ± 0.24	0.16 ± 0.02
X-407/CTAB (Fresh)	2.11 ± 0.15	4.67 ± 0.26	8.12 ± 0.43	0.26 ± 0.03
X-407/CTAB (Aged 180°C)	2.45 ± 0.21	6.32 ± 0.42	11.25 ± 0.65	0.35 ± 0.04

3.5.3 Bulk-Scale Architecture: Weak 3D Network and Isotropic Suspension

The excellent and angle-independent sag resistance is facilitated by the formation of a weak, yet pervasive, three-dimensional network within the continuous oil phase. The hyperbranched architecture of HP-Wet promotes intermolecular interactions through chain entanglement and possible hydrogen bonding. The introduction of CTAB amplifies this networking through electrostatic cross-linking (each CTAB molecule can interact with multiple cationic sites on different HP-Wet molecules) and hydrophobic chain association. This network manifests macroscopically as a significant and stable YP. It acts as a uniform, isotropic scaffold that provides consistent gel strength throughout the fluid, effectively suspending the oleophilically-modified barite particles against gravitational settling regardless of wellbore deviation. This mechanism is the direct cause of the superior SF maintained at 0°, 45°, and 90° inclinations (Fig. 7b).

3.5.4 Integrated Consequence: From Particle Stabilization to System-Wide Performance

The ultra-low HTHP FL and robust emulsion stability are integrated consequences of the above mechanisms. The stable emulsion with fine, uniform droplets (evidenced by droplet size analysis in Table 13) minimizes aqueous phase mobility. Simultaneously, the perfectly oleophilic and uniformly suspended barite particles contribute to forming a thin, low-permeability filter cake. The synergy between molecular anchoring, interfacial hydrophobic layer formation, and bulk-phase network construction collectively underpins the superior comprehensive performance, with sag prevention at its core.

4 Conclusions and Recommendations

4.1 Conclusions

A novel hyperbranched polymeric wetting agent (HP-Wet) was successfully synthesized via a molecular topology strategy aimed specifically at solid-phase control in ultra-low OWR OBDFs. Unlike conventional emulsifiers that stabilize the oil—water interface, HP-Wet incorporates phosphonate groups that anchor strongly onto barite surfaces, complemented by long alkyl chains that confer oleophilicity. When synergized electrostatically with CTAB, HP-Wet fundamentally and durably reverses barite wettability, increasing the water contact angle from 21.9° to over 117.1°. At an ultra-low OWR of 55:45 and after dynamic aging at 180°C, the HP-Wet/CTAB system delivers outstanding sag resistance (SF = 0.505), a high electrical stability (>1000 V), and an ultra-low HTHP fluid loss (1.5 mL). These values significantly outperform those of a commercial wetting agent X-407 (SF = 0.517, ES = 915 V, HTHP FL = 2.6 mL). The enhanced performance stems from a multi-scale mechanism distinct from interfacial emulsification:

(1) molecular-scale chelation of phosphonate groups with surface Ba^{2+} ions and electrostatic locking by CTAB;
(2) Formation of a dense, thermally self-reinforcing hydrophobic shell at the solid–oil interface; a
(3) Construction of a weak three-dimensional network in the continuous phase that provides uniform, angle-independent particle suspension.

This work not only presents a high-performance, environmentally compatible additive (EC_{50} = 37,600 mg/L, non-toxic) but, more importantly, establishes a new molecular design paradigm focused on solid-phase wettability control and sag prevention. By directly addressing the root cause of barite sag—surface hydrophilicity—rather than relying solely on bulk rheology or interfacial film strength, our approach offers a complementary and more targeted solution for stabilizing advanced OBDFs under extreme downhole conditions.

4.2 Limitations and Future Perspectives

While this study provides strong correlative evidence for the proposed multi-scale sag control mechanism through macroscopic performance, wettability, and colloidal characterization, direct microstructural visualization of the adsorbed polymer layer and the 3D network remains a limitation. The hyperbranched architecture and phosphonate incorporation are supported by FTIR, GPC, zeta potential, wettability, and ^{1}H NMR. However, due to molecular aggregation in common NMR solvents, the ^{1}H NMR spectrum exhibits severe peak broadening, precluding reliable determination of the degree of branching (DB). Attempts at ^{31}P NMR were similarly hampered. To furnish more conclusive evidence and deepen mechanistic understanding, future work will focus on:

(1) Solid-state ^{31}P NMR or synthesis of a lower-molecular-weight HP-Wet analog to enable conventional high-resolution NMR for quantitative DB assessment.
(2) Direct visualization of the HP-Wet/CTAB adsorption layer on barite surfaces and the network structure using cryo-SEM or AFM.
(3) High-temperature interfacial rheology or *in situ* scattering to directly probe the proposed thermally induced reinforcement of the interfacial film.
(4) Pilot-scale synthesis and controlled field trials to validate practical performance and economic feasibility under real drilling conditions.

Acknowledgement: None.

Funding Statement: This work was supported by Applied Technology Research and Development Program Project in Heilongjiang Province (GA20A201).

Author Contributions: Conceptualization, Dapeng Zou, Jun Wang; data curation, Dapeng Zou; writing—original draft preparation, Dapeng Zou; formal analysis, Dapeng Zou; writing—review and editing, Dapeng Zou. All authors reviewed the results and approved the final version of the manuscript. All authors reviewed and approved the final version of the manuscript.

Availability of Data and Materials: The data that support the findings of this study are available from the corresponding author upon reasonable request.

Ethics Approval: Not applicable.

Conflicts of Interest: The authors declare no conflicts of interest. Dapeng Zou is employed by Drilling Fluid Company, Daqing Drilling & Exploration Engineering Corporation. This affiliation did not influence the design, execution, analysis, or interpretation of the data, nor the decision to publish.

References

1. Sun J, Xu G, Ding Y, Lyu K, Fan J, Li J. Advances and future prospects of shale oil and gas drilling fluid technology. Petrol Explor Dev. 2025;52(6):1609–23. doi:10.1016/S1876-3804(26)60665-9.
2. Song HX, Zhang SL, Chen XW, Wyclif K, Guo JX, Xiong RY, et al. Research on the pollution and damage mechanism of drilling fluid on casing during ultra-deep well drilling process. Petrol Sci. 2025;22(3):1234–51. doi:10.1016/j.petsci.2024.12.019.
3. She C, Guo J, Tang Y, Wang Y, Zhang YT, Wang J. Poly(vinyl alcohol)-doped surface-modified graphene oxide/cellulose porous aerogel for oil-based drilling fluid plugging. ACS Omega. 2025;10(4):3665–75. doi:10.1021/acsomega.4c08688.
4. Ao H, Lin L, Pu D, Zhang X, Luo Y, Wang M, et al. Synthesis and performance evaluation of a modified acrylate flocculant SDCD for waste oil-based drilling fluid. J Appl Polym Sci. 2025;142(24):e57031. doi:10.1002/app.57031.

5. Ma J, Xia B, An Y. Advanced developments in low-toxic and environmentally friendly shale inhibitor: a review. J Petrol Sci Eng. 2022;208(1):109578. doi:10.1016/j.petrol.2021.109578.
6. Yang J, Sun J, Wang R, Qu Y. Treatment of drilling fluid waste during oil and gas drilling: a review. Environ Sci Pollut Res. 2023;30(8):19662–82. doi:10.1007/s11356-022-25114-x.
7. Lysakova EI, Skorobogatova AD, Shashkova TL, Grigoriev YS, Neverov AL, Pryazhnikov MI. Environmentally friendly technical plant oils as the base for emulsion drilling fluids. Emergent Mater. 2025;8(3):2307–24. doi:10.1007/s42247-024-00944-2.
8. Li S, Xia BR, Han XZ, Wang XG, Li ZJ. Effects of oil-water ratio on performance of oil-based drilling fluid. Oilfield Chem. 2017;34(2):196–200. (In Chinese). doi:10.19346/j.cnki.1000-4092.2017.02.002.
9. Fu SL, Hou SS, Wu Y, You FC, He M. Analysis of factors affecting stability of low oil-water ratio Emulsion. Oilfield Chem. 2021;38(2):191–5 215. (In Chinese). doi:10.19346/j.cnki.1000-4092.2021.02.001.
10. Xiao X, Xu MB, You FC, Fan YG, Wang XL, Zhou J. Influence factor of filtration property of oil-based drilling fluid with different oil-water ratio. Oilfield Chem. 2018;35(4):577–81. (In Chinese). doi:10.19346/j.cnki.1000-4092.2018.04.002.
11. Basfar S, Shokry A, Iqbal A, Elkatatny S, Alajmi S. Evaluation of the effects of Kaolin clay on the performance of barite-weighted oil-based drilling fluid. ACS Omega. 2025;10(10):9976–85. doi:10.1021/acsomega.4c07376.
12. Khalili P, Khalifeh M, Saasen A, Naccache M. Rheological compatibility of a hardening spacer fluid and oil-based drilling fluid. SPE J. 2023;28(6):2845–60. doi:10.2118/217446-PA.
13. Ghasemi M, Moslemizadeh A, Shahbazi K, Mohammadzadeh O, Zendehboudi S, Jafari S. Primary evaluation of a natural surfactant for inhibiting clay swelling. J Petrol Sci Eng. 2019;178(3):878–91. doi:10.1016/j.petrol.2019.02.073.
14. Hajiabadi SH, Bedrikovetsky P, Mahani H, Khoshsima A, Aghaei H, Kalateh-Aghamohammadi M, et al. Effects of surface modified nanosilica on drilling fluid and formation damage. J Petrol Sci Eng. 2020;194(2):107559. doi:10.1016/j.petrol.2020.107559.
15. Jiang G, Ni X, Yang L, Li W, Li Y, Deng Z. Synthesis of superamphiphobic nanofluid as a multi-functional additive in oil-based drilling fluid, especially the stabilization performance on the water/oil interface. Colloids Surf A Physicochem Eng Aspects. 2020;588(18):124385. doi:10.1016/j.colsurfa.2019.124385.
16. Kadirgama K. A comprehensive review on the application of nanofluids in the machining process. Int J Adv Manuf Technol. 2021;115(9):2669–81. doi:10.1007/s00170-021-07316-8.
17. Ospanov YK, Kudaikulova GA. Synergistic effects of graphene oxide and nanocellulose on water-based drilling fluids: improved filtration and shale stabilization. Polymers. 2025;17(7):949. doi:10.3390/polym17070949.
18. Kiiza J, Xu J. Functional groups optimization at molecular-scale to improve polyamine treatment agent performance on sodium bentonite surface hydration inhibition under high-temperature/high-pressure failure. Chem Phys. 2025;594(44):112649. doi:10.1016/j.chemphys.2025.112649.
19. Xu C, Yan F, Wang M, Yan H, Cui Z, Li J, et al. Fabrication of hyperbranched polyether demulsifier modified PVDF membrane for demulsification and separation of oil-in-water emulsion. J Membr Sci. 2020;602:117974. doi:10.1016/j.memsci.2020.117974.
20. Lim YW, Bell CA, Fletcher NL, Condon ND, Akhter DT, Rae J, et al. Trans-endothelial trafficking in zebrafish: nanobio interactions of polyethylene glycol-based nanoparticles in live vasculature. ACS Nano. 2026;20(3):3132–55. doi:10.1021/acsnano.5c21042.
21. Fu Y, Li H, Liu C, Tian W. Chemical reactions in living cells for enhanced biological treatment. Chin Chemical Lett. 2026;37(4):112220. doi:10.1016/j.cclet.2025.112220.
22. Hu Q, Chen H, Cheng H, Zhang J, Shi X, Gao C. Biocompatible and antibacterial polymers for biomedical applications: a minireview. Biomed Mater. 2026;21(1):012003. doi:10.1088/1748-605X/ae2a8c.
23. De B, Bera M, Bhattacharjee D, Ray BC, Mukherjee S. A comprehensive review on fiber-reinforced polymer composites: raw materials to applications, recycling, and waste management. Prog Mater Sci. 2024;146(2):101326. doi:10.1016/j.pmatsci.2024.101326.
24. Wang Y, Qiu X, Wu C, Li J, Dai C, Han B, et al. Reactive integration of amino-functional 9, 10-dihydro-9-oxa-10-phosphaphenanthrene-10-oxide (DOPO)-modified metal–organic frameworks (MOFs) into polyurea balancing flame retardancy and mechanical properties. J Polym Mater. 2026;43(1):8. doi:10.32604/jpm.2026.076443.

25. Bi L, Yang L, Bhunia AK, Yao Y. Emulsion stabilized with phytoglycogen octenyl succinate prolongs the antimicrobial efficacy of ε-poly-l-lysine against *Escherichia coli* O157:H7. LWT. 2016;70(No. 2):245–51. doi:10.1016/j.lwt.2016.02.049.
26. Huang Y, Qiao C, Li Z, Zeng H. Mechanistic insights into the role of branched polyethylenimine in breaking asphaltene-stabilized oil-in-water emulsions: temperature effects. Sep Purif Technol. 2025;362(9):131913. doi:10.1016/j.seppur.2025.131913.
27. Sun Q, Qiu ZS, Geng T, Zhong HY, Liu W, Tang YL, et al. Application of a hyperbranched amide polymer in high-temperature drilling fluids: inhibiting barite sag and action mechanisms. J Polym Mater. 2025;42(3):757–72. doi:10.32604/jpm.2025.069808.
28. Wang J, Xu M, Xiao W. Synergistic emulsifier system based on molecular design for ultra-low oil-to-water ratio oil-based drilling fluids. J Polym Mater. 2026;43(1):14. doi:10.32604/jpm.2026.077100.
29. API RP 13B-1-2019. API recommended practice for standard procedure for testing drilling fluid. Houston, TX, USA: American Petroleum Institute; 1974.
30. Rafati R, Smith SR, Sharifi Haddad A, Novara R, Hamidi H. Effect of nanoparticles on the modifications of drilling fluids properties: a review of recent advances. J Petrol Sci Eng. 2018;161(7):61–76. doi:10.1016/j.petrol.2017.11.067.
31. Magalhães SC, Calçada LA, Scheid CM, Almeida H, Waldmann ATA. Improving drilling performance with continuous online measurements of electrical stability and conductivity in oil based drilling fluids. J Petrol Sci Eng. 2016;146(14):369–79. doi:10.1016/j.petrol.2016.05.045.
32. Yang J, Wang R, Dong B, Ai Z, Peng L, Xie G. Investigating on the performance and mechanism of poly(styrene-methyl methacrylate-ethyl methacrylate-butyl acrylate) as nano sealing agent in oil-based drilling fluids. ACS Omega. 2024;9(40):41250–7. doi:10.1021/acsomega.4c03083.
33. Maxey J. Rheological analysis of static and dynamic sag in drilling fluids. In: Proceedings of the Nordic Rheology Conference; 2007 Jun 13–15; Stavanger, Norway.
34. Huang X, Sun J, Lyu K, Dong X, Liu F, Gao C. A high-temperature resistant and high-density polymeric saturated brine-based drilling fluid. Petrol Explor Dev. 2023;50(5):1215–24. doi:10.1016/S1876-3804(23)60460-4.
35. Li XL, Jiang GC, Xu Y, Deng ZQ, Wang K. A new environmentally friendly water-based drilling fluids with laponite nanoparticles and polysaccharide/polypeptide derivatives. Petrol Sci. 2022;19(6):2959–68. doi:10.1016/j.petsci.2022.07.003.
36. Wang L. Preparation and application of viscosifier for environmentally friendly oil-based drilling fluid. Chem Technol Fuels Oils. 2015;51(5):539–44. doi:10.1007/s10553-015-0637-2.
37. Sanders PF, Tibbetts PJC. Effects of discarded drill muds on microbial populations. Philos Trans R Soc Lond B Biol Sci. 1987;316(1181):567–85. doi:10.1098/rstb.1987.0039.
38. Alabarse FG, Conceição RV, Balzaretti NM, Schenato F, Xavier AM. *In-situ* FTIR analyses of bentonite under high-pressure. Appl Clay Sci. 2011;51(1–2):202–8. doi:10.1016/j.clay.2010.11.017.
39. Liu L, Pu X, Zhou Y, Zhou J, Luo D, Ren Z. Smart pickering water-in-oil emulsion by manipulating interactions between nanoparticles and surfactant as potential oil-based drilling fluid. Colloids Surf A Physicochem Eng Aspects. 2020;586:124246. doi:10.1016/j.colsurfa.2019.124246.
40. Ma XY, Wang XC, Ngo HH, Guo W, Wu MN, Wang N. Bioassay based luminescent bacteria: interferences, improvements, and applications. Sci Total Environ. 2014;468–469:1–11. doi:10.1016/j.scitotenv.2013.08.028.
41. Yang X, Shang Z, Liu H, Cai J, Jiang G. Environmental-friendly salt water mud with nano-SiO_2 in horizontal drilling for shale gas. J Petrol Sci Eng. 2017;156(1):408–18. doi:10.1016/j.petrol.2017.06.022.
42. Zhang H, Gao J, Wang H, Chen H, Dai H, Ma L, et al. Effect of tannic acid on the heat-induced flocculation of gelatin/cellulose nanocrystal-based emulsions: mechanisms behind the formation of high internal phase emulsion gels. Food Hydrocoll. 2026;170(2):111765. doi:10.1016/j.foodhyd.2025.111765.
43. Kim DH. Regioisomeric effect on the stereoscopic conformational transition of polymer monolayers at the aqueous interface. J Phys Chem Lett. 2025;16(9):2160–5. doi:10.1021/acs.jpclett.5c00069.
44. Maldonado-Valderrama J, del Castillo-Santaella T, Adroher-Benítez I, Moncho-Jordá A, Martín-Molina A. Thermoresponsive microgels at the air–water interface: the impact of the swelling state on interfacial conformation. Soft Matter. 2017;13(1):230–8. doi:10.1039/C6SM01375A.